Article

TRANSPARENT PROCESS OPEN ACCESS

THE EMBO JOURNAL

Local rewiring of genome–nuclear lamina interactions by transcription

Laura Brueckner[1], Peiyao A Zhao[2], Tom van Schaik[1], Christ Leemans[1], Jiao Sima[2], Daniel Peric-Hupkes[1], David M Gilbert[2] & Bas van Steensel[1,3,*]

Abstract

Transcriptionally inactive genes are often positioned at the nuclear lamina (NL), as part of large lamina-associated domains (LADs). Activation of such genes is often accompanied by repositioning toward the nuclear interior. How this process works and how it impacts flanking chromosomal regions are poorly understood. We addressed these questions by systematic activation or inactivation of individual genes, followed by detailed genome-wide analysis of NL interactions, replication timing, and transcription patterns. Gene activation inside LADs typically causes NL detachment of the entire transcription unit, but rarely more than 50–100 kb of flanking DNA, even when multiple neighboring genes are activated. The degree of detachment depends on the expression level and the length of the activated gene. Loss of NL interactions coincides with a switch from late to early replication timing, but the latter can involve longer stretches of DNA. Inactivation of active genes can lead to increased NL contacts. These extensive datasets are a resource for the analysis of LAD rewiring by transcription and reveal a remarkable flexibility of interphase chromosomes.

Keywords genome organization; lamina-associated domains; nuclear lamina; replication timing; transcription

Subject Category Chromatin, Transcription & Genomics

DOI 10.15252/embj.2019103159 | Received 6 August 2019 | Revised 23 January 2020 | Accepted 28 January 2020 | Published online 21 February 2020

The EMBO Journal (2020) 39: e103159

Introduction

In metazoan cell nuclei, large chromatin domains are associated with the nuclear lamina (NL) (Gonzalez-Sandoval & Gasser, 2016; van Steensel & Belmont, 2017; de Leeuw *et al*, 2018; Kim *et al*, 2019; Lochs *et al*, 2019). Mammalian genomes have roughly one thousand of such lamina-associated domains (LADs), which are typically hundreds of kb or even a few Mb in size. The NL contacts of some LADs are highly consistent between cell types, while other LADs interact in cell-type-specific (facultative) manners with the NL. How LAD-NL contacts are regulated is poorly understood.

Most genes inside LADs have very low transcriptional activity (Guelen *et al*, 2008; Peric-Hupkes *et al*, 2010; Leemans *et al*, 2019). When cells differentiate, detachment of genes from the NL often coincides with transcriptional activation, while increased NL interactions correlate with reduced transcription (Peric-Hupkes *et al*, 2010; Lund *et al*, 2013; Robson *et al*, 2016, 2017). These observations raise the interesting possibility that the NL helps to establish a repressive environment. In support of this notion, depletion of lamins can lead to derepression of specific genes (primarily in *Drosophila*) (Shevelyov *et al*, 2009; Kohwi *et al*, 2013; Chen *et al*, 2014); transfer of human inactive promoters from LADs to a neutral chromatin environment can lead to activation of these promoters (Leemans *et al*, 2019); and artificial tethering of some genes to the NL can reduce their activity (Finlan *et al*, 2008; Kumaran & Spector, 2008; Reddy *et al*, 2008; Dialynas *et al*, 2010).

This, however, does not rule out that the contacts of genes with the NL are the *consequence* of a lack of transcriptional activity, and vice versa, that genes detach from the NL *in response* to their activation. This was initially suggested by experiments with fluorescently tagged lacO arrays that were integrated in a locus near the NL. Tethering of the transcriptional activator peptide VP16 to these arrays caused repositioning away from the NL (Tumbar & Belmont, 2001). Similar observations were made when VP64 (a tetramer of VP16) was tethered to promoters of three distinct genes in LADs in mouse embryonic stem (mES) cells (Therizols *et al*, 2014). Another study found that activation of the long non-coding RNA gene *ThymoD* in mouse T-cell progenitors contributed to the detachment of the neighboring gene *Bcl11b* from the NL (Isoda *et al*, 2017). The molecular signals that cause detachment of a locus from the NL are still poorly understood.

Analysis of NL detachment that follows forced activation of a gene has so far been limited to a handful of loci. It is thus unclear whether the observed detachment from the NL after transcription activation is universal, or limited to genes with particular features. For example, do the size of the gene and its level of transcription matter? Moreover, the previous studies of individual loci have only been based on microscopy-based assays such as fluorescence *in situ* hybridization (FISH) or LacO tagging and have only visualized the targeted genes

1 Division of Gene Regulation and Oncode Institute, Netherlands Cancer Institute, Amsterdam, The Netherlands
2 Department of Biological Science, Florida State University, Tallahassee, FL, USA
3 Department of Cell Biology, Erasmus University Medical Center, Rotterdam, The Netherlands
*Corresponding author. Tel: +31-20-5122040; E-mail: b.v.steensel@nki.nl

themselves, but not the flanking DNA sequences. It has therefore remained unclear what the impact of these repositioning events is on the surrounding chromosomal regions. One possible scenario is that activation of a single gene inside a LAD leads to movement of the whole surrounding LAD to the nuclear interior. Alternatively, detachment could be restricted to the target gene itself or only affect some of its flanking regions. Possibly, detachment of one locus from the NL could be compensated by increased NL contacts of another locus nearby. To investigate this, high-resolution maps of NL interactions after manipulation of the activity of individual genes are needed.

Nuclear lamina interactions have also been associated with the timing of DNA replication during S-phase. LADs typically coincide with late-replicating domains, but the overlap is not complete, particularly at the edges of LADs (Guelen *et al*, 2008; Peric-Hupkes *et al*, 2010; Pope *et al*, 2014). These local discrepancies are still poorly understood, but may provide important clues about the interplay between the mechanisms that establish LADs and late-replicating domains. Above-mentioned activation of genes in LADs with TALE-VP64 was accompanied by a switch from late to early replication; however, it was not analyzed how far this switch extends across the locus and how well it tracks with the changes in NL contacts (Therizols *et al*, 2014).

To study these issues, we took three complementary approaches. First, we used two VP16-tethering methods to activate a total of 14 different genes inside LADs, querying a variety of gene contexts. Second, we inactivated or truncated selected genes genetically to test whether they would re-attach to the NL. Third, we integrated an active transgene driven by a strong promoter into multiple LADs and tested how this altered NL interactions of the integration sites and the flanking regions. In each instance, we used DamID to map NL interactions, enabling us to visualize the extent of NL detachment in detail along entire chromosomes. We also compared the changes in NL interactions to changes in replication timing.

Results

Detachment of genes from the NL upon activation by TALE-VP64

We first employed a previously reported system in mouse embryonic stem (ES) cells, in which individual NL-associated genes are upregulated by means of TALE-VP64 fusion proteins that target the promoters (Therizols *et al*, 2014). In this system, relocation of the activated genes from the NL toward the nuclear interior was observed by FISH (Therizols *et al*, 2014). However, it is not known how much of the flanking DNA is involved in this detachment from the NL. We therefore repeated these experiments, but now we employed DamID mapping of lamin B1 interactions. This method has repeatedly been shown to correspond well with FISH microscopy (Guelen *et al*, 2008; Peric-Hupkes *et al*, 2010; Harr *et al*, 2015; Kind *et al*, 2015; Robson *et al*, 2017), but it provides much more detailed maps of NL interactions.

We focused on two previously studied genes, *Sox6* and *Nrp1* (Therizols *et al*, 2014). In line with the reported FISH results, we observed clear detachment of each gene from the NL, when activated by the corresponding TALE-VP64 construct (Fig 1A and B middle panels). To assess the statistical significance of these changes, we compared their magnitude to those observed throughout the remainder of the genome. Because the size of the affected region is *a priori* not known, we calculated this comparison for various window sizes between about 30 kb and 1 Mb. This resulted in domainograms (de Wit *et al*, 2008; Tolhuis *et al*, 2011) that depict the genome-wide ranking of displacement magnitudes as a function of window position as well as window size (Fig 1A and B top panels; see Appendix Fig S1 for an explanation of domainograms). We regard displacements that rank above the 95th percentile or below the 5th percentile (marked in shades of blue and red for decreased and increased NL interactions, respectively) and that occur locally near the targeted gene, to be highly likely due to direct effects. We note that some indirect displacements elsewhere in the genome may be expected, because the perturbations of *Sox6* and *Nrp1* may have secondary effects on gene expression.

The domainograms indicate that the displacements of the respective targeted genes were among the most extreme throughout the genome. For *Sox6,* the NL detachment included the entire gene, but it was more pronounced near the promoter than toward the 3′ end (Fig 1A). Upstream of the promoter the detachment extended over ~50–100 kb, up to the LAD border. Downstream of the gene, a modest detachment was observable that tapered off over ~300 kb. Interestingly, about 0.5 Mb upstream, across the LAD border, also some reduction in NL interactions is visible. For *Nrp1,* the detachment also involved the entire gene body but did not extend much beyond it (Fig 1B). We note that the loss of DamID signal along active transcription units cannot be attributed to the RNA polymerase machinery blocking access to Dam methylation, because all DamID data are normalized to a Dam-only control that corrects for such accessibility biases (Greil *et al*, 2006), and the same experimental design has successfully detected interaction of specific proteins with actively transcribed regions (Filion *et al*, 2010). About 180 kb downstream of *Nrp1*, the gene *Itgb1* showed a modest increase in NL interactions. This will be discussed below. Together, these data show that activation of two genes inside LADs of mES cells results in detachment from the NL along the entire gene body, possibly with some subtler involvement of flanking regions.

Detachment span is linked to transcript length

To extend this analysis to a larger number of genes, we switched to a more flexible gene activation system that does not require a custom-made TALE for every promoter of interest. We chose a previously established human RPE-1 cell line that stably expresses the SunCas-CRISPRa system (Tanenbaum *et al*, 2014; Tame *et al*, 2017), in which multiple copies of VP64 can be targeted to a promoter of interest by a single sgRNA. We first used this system to activate *NLGN1*, a gene of 885 kb that is located in a LAD. Transfection with a sgRNA targeting the promoter caused ~80-fold upregulation (Appendix Fig S2) and resulted in clear detachment from the NL (Fig 2A). Relocalization primarily affected the *NLGN1* gene itself, with a mild 5′ to 3′ gradient inside the gene body and gradually decreasing along ~100 kb of flanking DNA. We also activated the *SOX6* gene in RPE-1 cells. Here, we activated one of the known alternative promoters located internally in the gene. Although the magnitude of the detachment was more modest, this gene also showed loss of NL interactions, but only downstream of the activated promoter (Fig 2B).

We applied this analysis in RPE-1 cells to 12 individual genes (Table 1) for which activation by the SunCas system could be

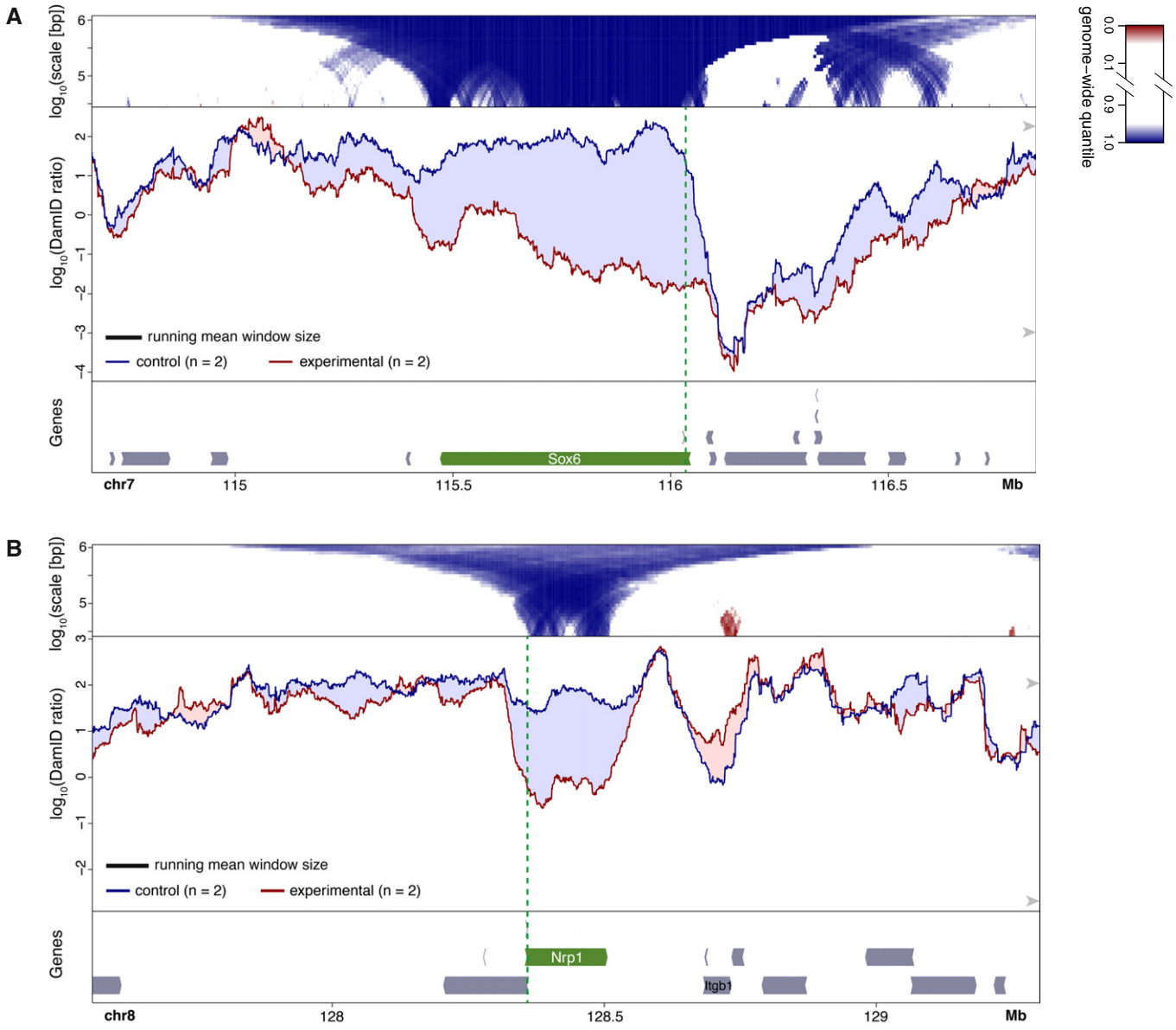

Figure 1. Changes in NL interactions of *Sox6* (A) and *Nrp1* (B) in mES cells after activation by TALE-VP64.

A, B *Bottom panels*: gene annotation track (mm10); the activated gene is marked in green and the location of the TALE-VP64 target sequence is shown by the vertical dashed green line. *Middle panels*: DamID tracks of NL interactions in control cells ("control", blue line) and cells expressing TALE-VP64 ("experimental", red line). n indicates the number of independent biological replicates that were combined. Noise was suppressed by a running mean filter of indicated window size. Shading between the lines corresponds to the color of the sample with the highest value. Arrowheads on the right-hand side mark the 5th and 95th percentiles of genome-wide DamID values. *Top panels*: domainograms; for every window of indicated size (vertical axis) and centered on a genomic position (horizontal axis), the pixel shade indicates the ranking of the change in DamID score (experimental minus control) in this window compared to the genome-wide changes in DamID scores across all possible windows of the same size. Blue: DamID score is highest in control samples; red: DamID score is highest in experimental samples (color key on the right of panel (A)). In (A) activation of *Sox6* was the experimental perturbation, activation of *Nrp1* (which is located on a different chromosome) served as control; in (B) activation of *Nrp1* was the experimental condition and activation of *Sox6* served as control.

achieved, as determined by RT–qPCR (Appendix Fig S2) or RNA-seq (Fig EV1). We chose genes of a wide variety of lengths, from ~2 kb to ~1.5 Mb. In three cases (*ABCB1*, *SLC35F3, and SOX6*), we targeted a known alternative promoter located in the middle of the gene, instead of the promoter located most 5′. Strikingly, for all 12 activated genes we observed detachment of the entire region extending from the activated promoter to the 3′ end of the gene (Fig 2C). For most of the tested genes, detachment did not extend more than several tens of kb upstream of the activated promoter. A clear exception to this is *PTN*, which exhibited upstream detachment over nearly 0.5 Mb (see below). Likewise, for most activated genes the detachment did not extend more than 50–100 kb downstream of the 3′ end, although the precise range varied.

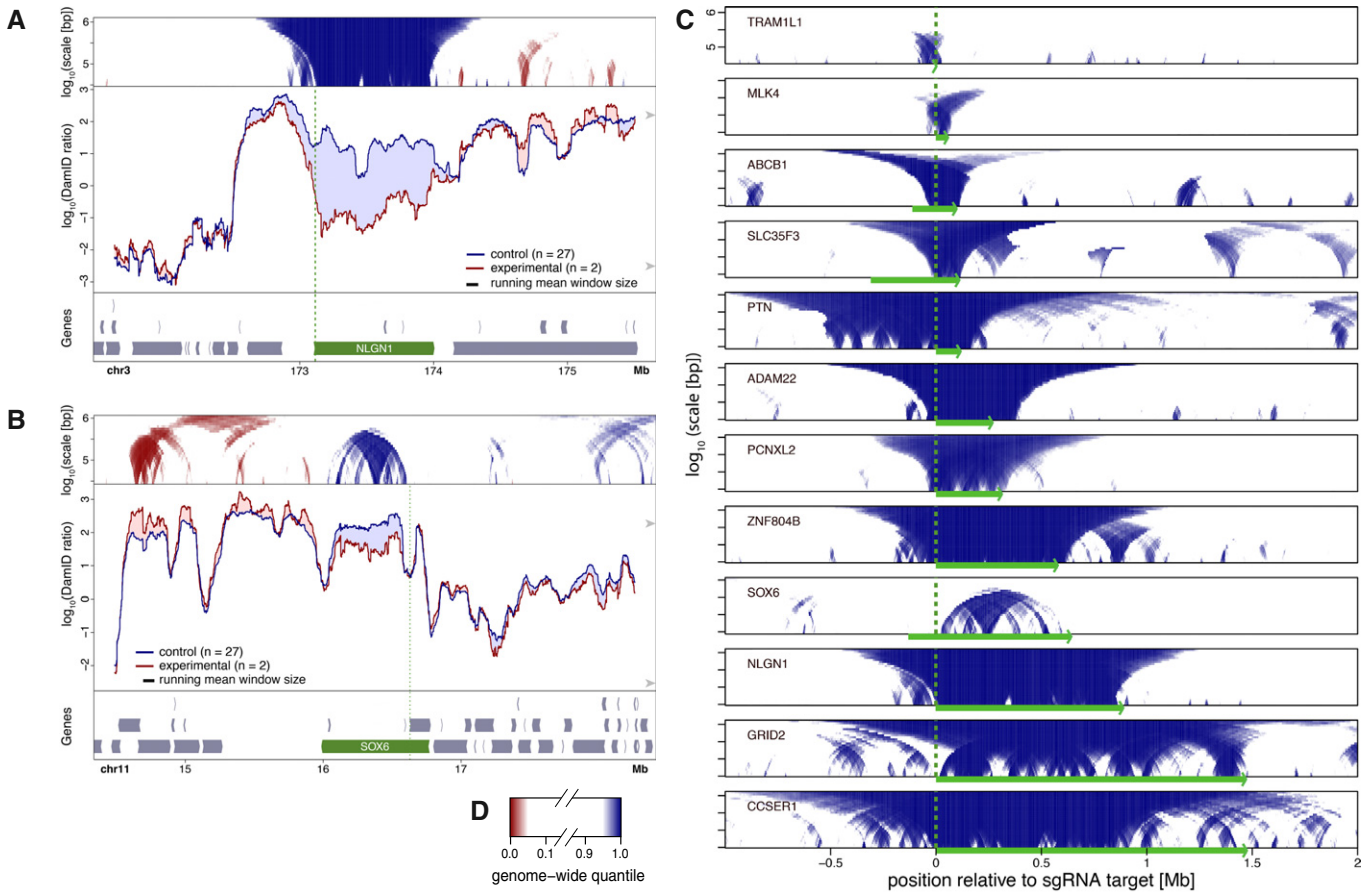

Figure 2. Local NL detachment caused by gene activation by CRISPRa in human RPE-1 cells.

A, B Plots as in Fig 1, showing changes in lamin B1 DamID signals upon CRISPRa activation of *NLGN1* (A) and *SOX6* (B). Control cells were treated either without sgRNA or with one of various sgRNAs targeting promoters on different chromosomes. Vertical green dotted lines mark the position of the sgRNA target sequence.

C Domainograms showing regions with reduced NL interactions around 12 genes individually activated by CRISPRa. Genomic regions are aligned by the respective sgRNA target positions and oriented so that the activated genes are all transcribed from left to right. Corresponding DamID traces are shown in Figs 2A and B, and 4, 5, EV2, EV4.

D Color key of domainograms in (A–C). Increases in NL interactions (red) are not shown in (C).

Quantitative link between gene expression level and NL detachment

We wondered whether the degree of NL detachment of a gene is quantitatively linked to the transcription level. To measure gene activity accurately, we performed RNA-seq after activation of 8 of the 12 genes and in the untreated parental cell line (Fig EV1). Comparing RNA levels and average DamID scores across the SunCas-activated genes before and after upregulation revealed a strong negative correlation (Fig 3). Thus, there is a remarkably quantitative inverse link between expression levels and NL interaction frequencies.

Neighboring genes of targeted genes do not generally show altered expression

We also queried our RNA-seq data for neighboring genes of the activated genes. We examined genes within ~1 Mb of our targets and generally could not detect substantial up- or downregulation (Fig EV1A–H). A notable exception is the gene *RUNDC3B* that is partially overlapping and antisense to the activated gene *ABCB1*. *RUNDC3B* is co-activated but does not show measurable detachment from the NL (Fig EV1A). Another, minor, exception is the gene *STEAP4* nearby the activated ADAM22 gene (Fig EV1B). In this case, the absolute expression level of this co-activated gene remained much lower than its CRISPRa-targeted neighbor. Thus, strong SunCas-induced upregulation is in most cases restricted to the targeted gene.

Some flanking genes co-detached from the NL together with the activated gene, but showed no detectable change in expression. The most striking example is the gene *DGKI* that flanks *PTN*. Much of this ~0.5 Mb gene shows reduced NL interactions upon activation of *PTN*, but *DGKI* does not undergo a detectable upregulation (Fig EV1G). We conclude that CRISPRa activation and the ensuing changes in NL contacts generally do not have substantial effects on the expression of nearby genes.

NL detachment partially overlaps with changes in replication timing

Next, we investigated the link between changes in NL interactions and replication timing. We applied Repli-seq (Marchal *et al*, 2018)

Table 1. Genes and sequences targeted by CRISPRa in RPE-1 cells.

Target gene	Target sequence	Target site (hg19)
ABCB1	GGGCCGGGAGCAGTCATCTG	chr7:87230290-87230310
ABCB4[a]	TGCAACGGTAGGCGTTTCCC	chr7: 87105074-87105093
ADAM22	CGGGCGACAAGAGCTCGGCA	chr7:87563472-87563492
CCSER1	GTGCGCGGAGTGTGACTGTG	chr4:91048592-91048612
GRID2	CAAAAGCATCCTGCAGCCTG	chr4:93225024-93225044
MLK4	AGGGCGGAATGAACCTGGAG	chr1:233463313-233463333
NLGN1	TGAAGGGTCAACCCTCCGCG	chr3:173115478-173115498
PCNX2	TCCCTCCTTAGCCTTCGCTG	chr1:233431545-233431565
PTN	GAGCAGAGGAAAATCCAAAG	chr7:137028354-137028374
RUNDC3B[a]	GCTGCTTTAAAAGGTCCGCG	chr7: 87257590-87257609
SLC35F3	TAAAGGGCTTCTCAGAGAGG	chr1:234349808-234349827
SOX6	GCTCCCCTCCCAGACAACAC	chr11:16629348-16629368
TRAM1L1	AGAATTCAGGAGCATCTTGG	chr4:118006859-118006879
ZNF804B	AGGCGCGGGTACCCATCGTC	chr7:88388864-88388884

[a]ABCB4 and RUNDC3B were only targeted in combination with ADAM22 and ABCB1.

to visualize replication timing, revisiting five genes that exhibited NL detachment in RPE-1 cells upon activation by CRISPRa. For all five activated genes, we observed a clear shift toward earlier replication. When the activated genes were relatively small (*ADAM22*, *ABCB1*, *PTN*), this shift was more or less symmetrical around the activated promoter and extended about 0.4–0.8 Mb on each side, i.e., well beyond the activated transcription units and also beyond the changes in NL interactions (Fig 4A–C). With longer activated genes (*CCSER1*, *GRID2*, both about 1.5 Mb long), again the shift in replication timing was strongest around the targeted promoter and extended about 0.6 Mb upstream (Fig EV2). Downstream of these promoters, the shift declined gradually toward the end of the gene, similar to the detachment from the NL.

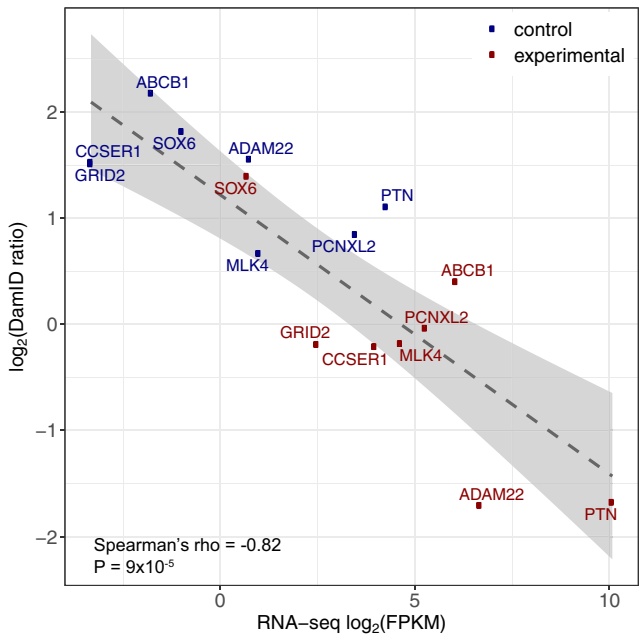

Figure 3. Inverse correlation between NL interaction and gene expression level in human RPE-1 cells.

Average DamID values plotted against average expression levels of eight genes activated by CRISPRa (red; $n = 2$) or in control cells that were treated either without sgRNA or with one of various sgRNAs targeting promoters on different chromosomes (blue; n ranging from 19 to 27).

We investigated whether the changes in NL interactions and replication timing were linked to topologically associated domains (TADs) as detected by the Hi-C technology (Dixon *et al*, 2012; Nora *et al*, 2012). For this, we analyzed previously reported Hi-C data from wild-type RPE-1 cells (Darrow *et al*, 2016; Data ref: Darrow *et al*, 2016). We focused on the *PTN* locus, which showed the most striking difference between the changes in NL contacts and Repli-seq patterns after CRISPRa. Interestingly, the change in Repli-seq pattern appeared not visibly linked to the (pre-existing) TAD pattern, while the changes in NL interactions showed a partial correlation with the TAD organization (Fig EV3). Together, these results reveal that changes in replication timing only partially overlap with changes in NL interactions (see Discussion).

Possible compensatory movements

In a few instances, we observed that the loss of NL interactions of the activated gene was accompanied by a gain of NL interactions of a nearby region. This was particularly notable for a region ~0.6 Mb downstream of the activated *MLK4* gene (Fig 5). This region coincides approximately with gene *SLC35F3*. The expression of *SLC35F3* is reduced by ~30% ($P = 0.02$, DESeq2 analysis) when *MLK4* was activated (Fig EV1E). Possibly, detachment of *MLK4* leads to compensatory movement of *SLC35F3* toward the NL, which in turn may contribute to slightly stronger repression of *SLC35F3*. Forced activation of *SLC35F3* caused its own NL detachment as expected (Fig 2C), but it did not alter the NL interactions of *MLK4* (Fig EV4A). This suggests that the putative compensatory relationship is not reciprocal, but we note that this latter experiment was done only once and should therefore be interpreted with caution.

We also observed moderately enhanced NL interactions of a region ~1.3 Mb downstream of the activated *SOX6* gene (Fig 2B). This region coincided with the promoters of two divergent genes that were not significantly up- or downregulated (Fig EV1H). Likewise, in case of *Nrp1* activated by TALE-VP64, the gene *Itgb1* (about 180 kb downstream of *Nrp1*) showed a modest increase in NL interactions (Fig 1B), but its expression was not found to be detectably altered by TALE-VP64 targeting of *Nrp1* (Therizols *et al*, 2014). We found also minor local increases in NL interactions within ~2 Mb of the activated genes *NLGN1* (Fig 2A), *TRAM1L1* and *ZNF804* (Fig EV4B and C). However, because of their modest magnitude, we did not further investigate these movements. In summary, possible compensatory changes in NL interactions around activated genes are relatively modest and may only anecdotally affect gene expression, at least in the cell systems we studied. These increases in NL interactions may reflect compensatory movement to fill up space at the NL vacated by the activated genes, but other secondary mechanisms cannot be ruled out.

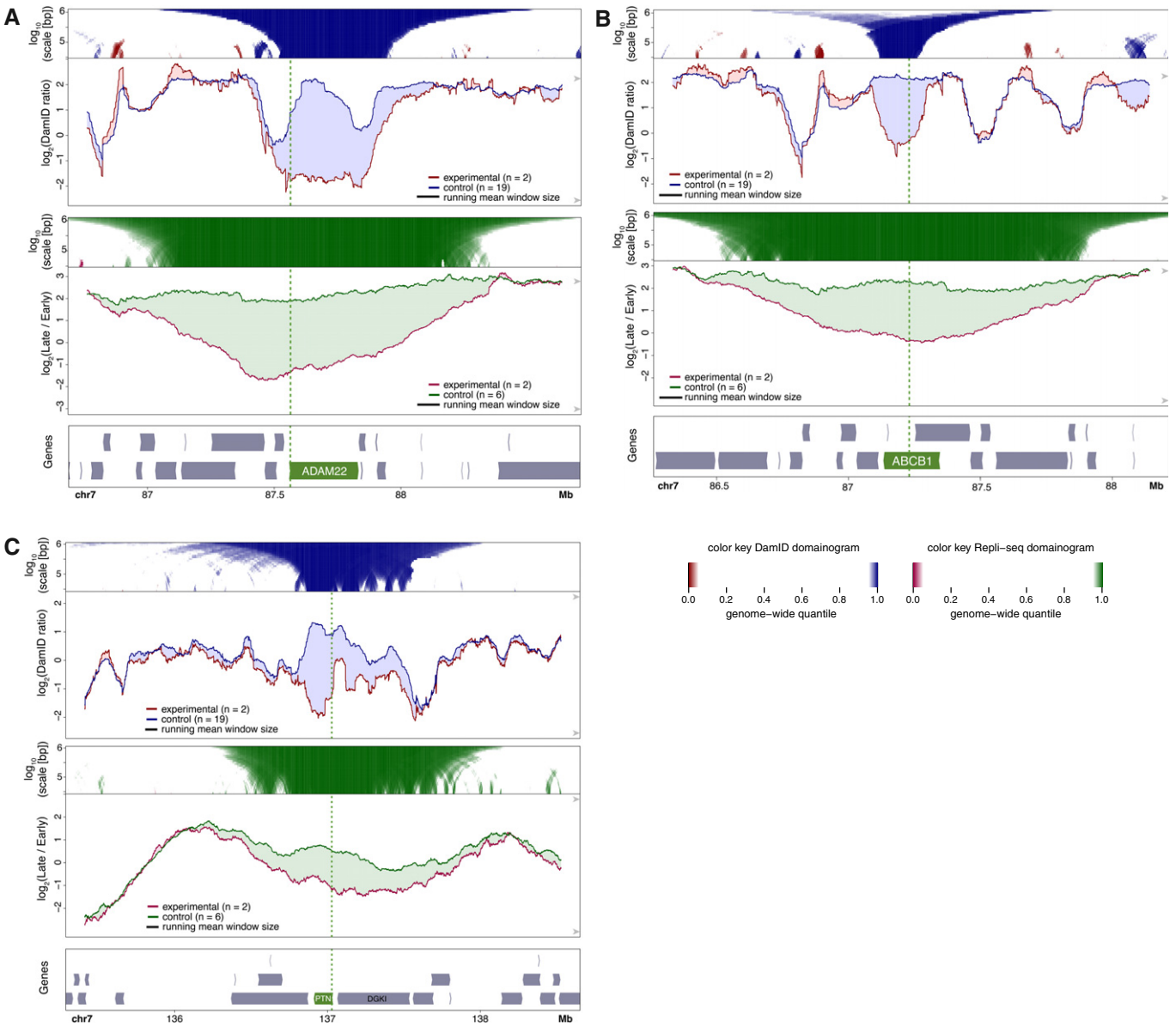

Figure 4. NL interactions and replication timing around activated genes.

A–C CRISPRa activation of *ADAM22* (A), *ABCB1* (B), and *PTN* (C) in human RPE-1 cells. Top panels visualize DamID data similar to Fig 2A and B. Middle panels show maps of replication timing at the same resolution and in the same plotting style as panels, except that different colors are used as indicated. Bottom panels show gene track, with activated gene highlighted in green.

Detachment remains local even if multiple genes are activated

We next explored whether it is possible to detach a whole LAD by activating multiple genes in the domain. We first tested this for two neighboring large genes, *CCSER1* (1,475 kb) and *GRID2* (1,468 kb). Activation of each gene individually caused clear detachment from the NL (Figs 6A and EV2A and B). When both genes were activated simultaneously (by co-transfection of the respective sgRNAs), both genes detached, but the intervening ~700 kb region showed no significant reduction in NL association (Fig 6A). Under this double-activating condition, the intervening region also continued to be replicated a bit later in S-phase than the two activated genes (Fig EV2C).

We also applied CRISPRa simultaneously to the much more closely spaced genes *ABCB4*, *ABCB1*, *ADAM22,* and *RUNDC3B* by co-transfection of four sgRNAs. All four genes were induced to varying levels (Fig EV5A and B). However, the activity of both *ABCB4* and *RUNDC3B* remained rather low under this quadruple activation condition, compared to their levels after CRISPRa of *ABCB1* alone (*cf*. Fig EV1A). This may be due to competition of the multiple sgRNAs for the available SunCas. We compared the resulting DamID maps to those obtained after activation of *ABCB1* or *ADAM22* alone (Figs 6B and EV5C–E). While the single gene activations resulted in selective detachment of the respective genes, the quadruple activation caused detachment of each gene, with the degree of detachment

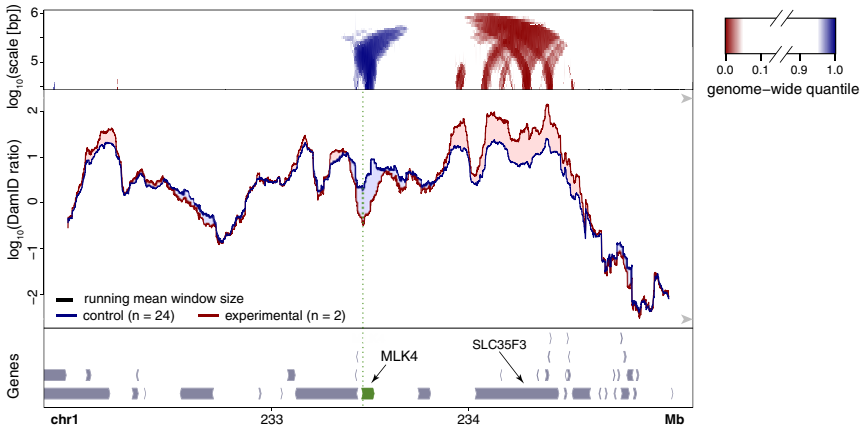

Figure 5. Putative compensatory movement near the activated *MLK4* gene.
Changes in NL interactions after CRISPRa activation of MLK4 in human RPE-1 cells. Visualization of DamID data as in Fig 2A and B.

roughly corresponding to the activity of each gene after activation (Fig EV5A and E). There was no indication that the observed detachment of the four genes involved a more extensive region than a simple combination of their independent detachments. However, it is noteworthy that the very modest activity of *ABCB4* and *RUNDC3B* after quadruple CRISPRa is sufficient to partially detach these two genes from the NL. This suggests that the detachment of these genes is facilitated by the detachment of the nearby *ABCB1* and *ADAM22* genes. Together, these results indicate that co-activation of multiple neighboring genes may lead to more efficient detachment of moderately active genes, but not to a broader detachment of flanking regions.

Inactivation of genes can promote NL interactions

Our observations so far strongly suggested that the act of transcription is a driving force that localizes genes to the nuclear interior. To test this further, we set out to block transcription by two complementary genetic strategies.

In the first strategy, we aimed to disrupt all transcription in an inter-LAD region (iLAD), to test whether this would lead to increased NL interactions of the entire region. We focused on the mouse genes *Dppa2, Dppa4, Morc1,* and *Morc* (a shorter form of *Morc1* that initiates from an alternative transcription start site). In ES cells, these genes are localized in an approximately 500 kb-sized iLAD. However, this region is NL-associated in mouse neural precursor cells (Peric-Hupkes *et al*, 2010), and therefore, it has the potential to become a LAD. We used recently reported (Sima *et al*, 2019) F1 hybrid *Cast/129Sv* mES cell clones (named E2 and A6) with a heterozygous triple deletion of the promoters of *DppA2, Morc1,* and *Morc* on the *129Sv*-derived chr16. These deletions also stop transcription of the *Dppa4* gene and therefore essentially abolish transcriptional activity in the whole iLAD (Sima *et al*, 2019). Owing to the high density of SNPs that differ between the *129Sv* and *Cast* genomes, we could generate allele-specific DamID maps, enabling us to compare the mutated and wild-type chromosomes.

DamID profiles of the locus revealed that *Morc1* and *Morc* on the mutated chromosome had moved toward the NL in the mutant cells, when compared to control cells carrying an unrelated mutation on a different chromosome (Fig 7A). This effect was not observed for the wild-type *Cast* chr16 in the same cells (Fig 7B). Interestingly, the region containing *Dppa2* and *Dppa4* was unaffected and clearly remained detached from the NL. This suggests that a transcription-independent detachment mechanism may exist in addition to a transcription-linked mechanism. To determine whether ablation of the most prominent transcript would be sufficient to induce attachment, we also tested a single deletion of the *Morc* promoter (clones A12 and B11), which reduces transcription of *Morc1* by ~2-fold and presumably ablates expression of *Morc,* but does not alter expression of *Dppa2* and *Dppa4* (Sima *et al*, 2019). In the mutated *129Sv*-derived locus, this perturbation resulted in a more restricted increase in NL interactions of *Morc* while the 5′ end of *Morc1* was much less affected (Fig 7C). Again, in the wild-type *Cast*-derived locus only minor changes were observed between mutated and control clones (Fig 7D). These data show that inactivation of one or more genes in a facultative iLAD can lead *in cis* to locally increased NL interactions of the inactivated genes.

In the second genetic approach, we aimed to truncate a single transcript, to test directly whether transcription elongation is required for detachment from the NL. We chose the 228 kb *Cobl* gene, which is active and locally detached from the NL in mES cells but inactive and NL-associated in neuronal precursor cells (NPCs), indicating that its detached state is facultative and linked to transcription. We created a heterozygous truncation of the *Cobl* transcription unit in F1 hybrid *Cast/129* mES cells by insertion of a polyadenylation sequence (PAS) in the *129* allele of *Cobl*, 89 kb downstream of the TSS. Analysis of *Cobl* allelic sequence variants in mRNA-seq data confirmed the premature termination of transcription at the *129Sv* allele (Appendix Fig S3). Allele-specific DamID profiles show increased NL interactions of the *129Sv* allele of *Cobl*, particularly downstream of the PAS integration (Fig 7E). This did not occur at the unmodified *CAST* allele, although some modest changes in NL interactions were detected in the surrounding region (Fig 7F). We conclude that blocking of *Cobl* transcription elongation causes local increases in NL interactions.

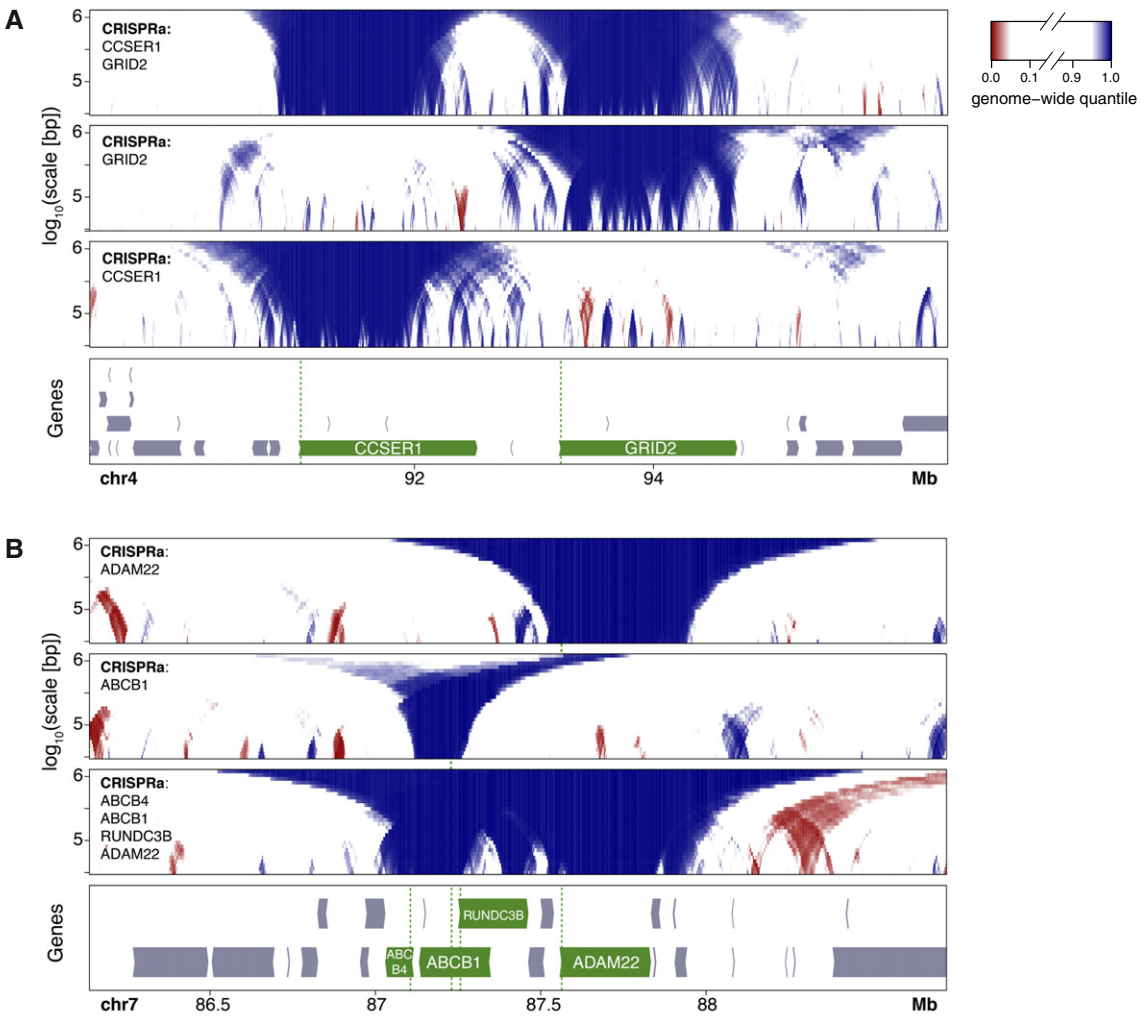

Figure 6. Effects of activation of multiple neighboring genes on NL interactions.

A DamID domainograms of NL interactions after activation of *CCSER1*, *GRID2*, or both.

B DamID domainograms after activation of ADAM22, ABCB1, or the genes *ABCB4*, *ABCB1*, ADAM22, and *RUNC3B* simultaneously.

Data information: All data are from human RPE-1 cells. DamID data of activation of *ADAM22* and *ABCB1* alone are same as in Fig 4A and B. See Figs EV2 and EV5 for additional visualization of these DamID data.

Insertion of a small active gene causes moderate detachment from the NL

Finally, complementary to the activation and inactivation of genes in their native context, we tested whether insertion of a highly active transgene into a LAD is sufficient to cause local detachment from the NL. For this purpose, we designed an expression cassette consisting of a transcription unit encoding enhanced green fluorescent protein (eGFP) driven by the strong human *PGK* promoter, cloned into a PiggyBac transposable element vector (Fig 8A). We integrated this cassette randomly in the genome of F1 hybrid mouse ES cells by co-transfection with PiggyBac transposase. We then isolated clonal cell lines and focused on two with a large number of integrations, reasoning that by random chance several integrations would occur inside LADs. Indeed, by inverse PCR and Tn5 mapping (see Materials and Methods) we found 17 uniquely mappable integrations to be inserted inside LADs, out of a total of 80 in the two cell clones combined (Fig 8B). In comparison with the corresponding wild-type alleles in the same cells, a roughly twofold reduction in average DamID signal was detected around the integration sites, spanning approximately 20 kb on each side (Fig 8C). We conclude that the integrated transcription units tend to detach the directly flanking DNA from the NL, but only partially and within a range of roughly 20 kb.

We considered the possibility that our expression cassette was not strong enough to cause more pronounced or extended detachments from the NL. To determine the expression level relative to endogenous genes, we performed RNA-seq and used the barcodes to estimate the expression levels of individual integrations (see Materials and Methods). Transcriptional activity was readily detectable for LAD integrations, although their median expression was about eightfold lower compared to the iLAD integrations (Fig 8D).

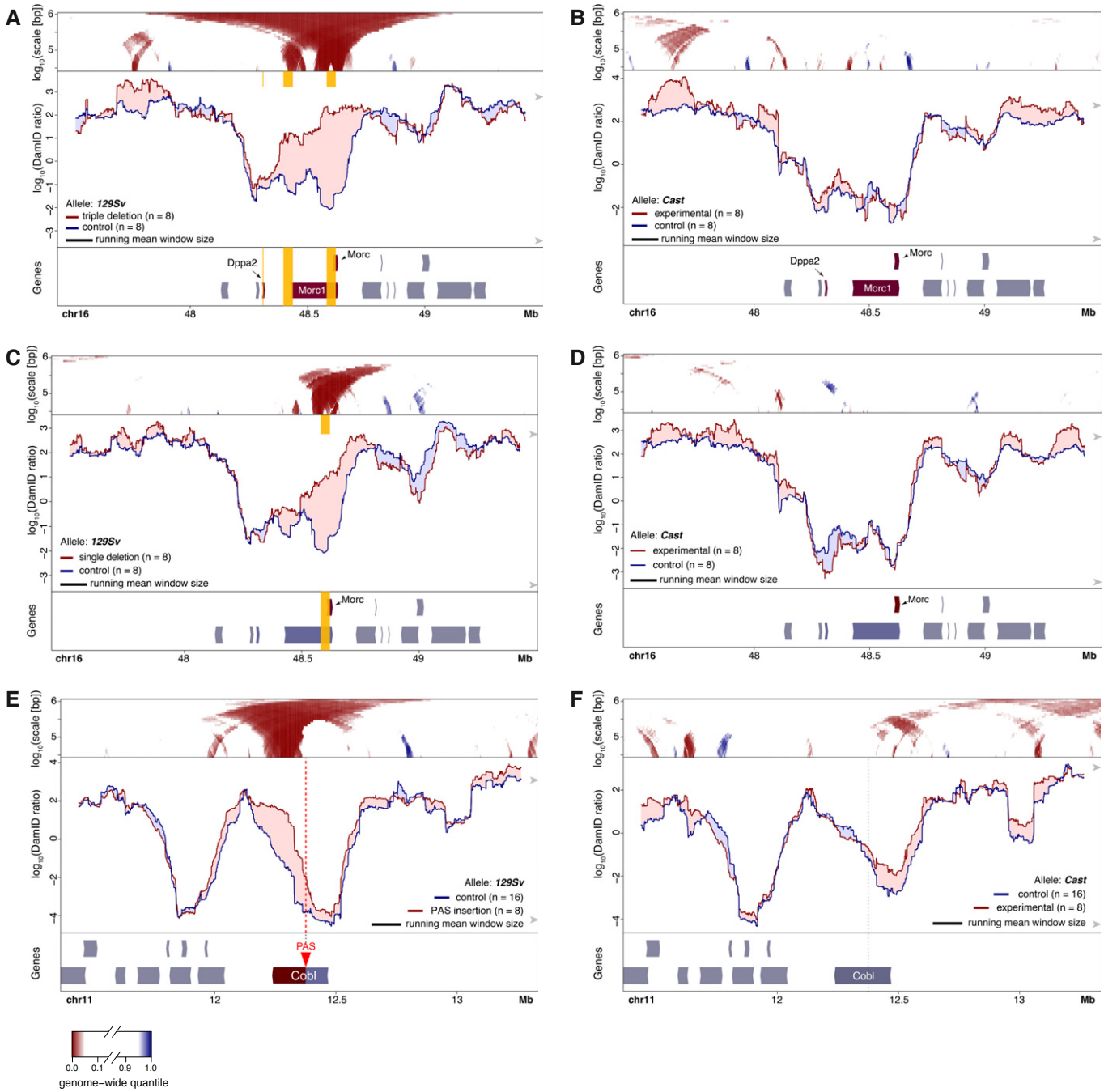

Figure 7. Increased NL interactions upon allele-specific transcription inactivation in F1 hybrid mES cells.

A DamID profiles of the *129Sv* allele of the *Morc1* locus with deletions of the promoters of *Morc*, *Morc1*, and *DppA2* (deletions marked by yellow vertical boxes) and in control cells.

B Same as (A), but for the non-mutated *Cast* allele.

C, D Same design as (A, B), but with only a single mono-allelic deletion of the *Morc* promoter (vertical yellow box).

E, F Effect of PAS insertion on NL interactions of *Cobl* gene locus. Same design as (A, B) but with insertion of a PAS (located at red triangle and vertical dotted line) that truncates the *129Sv* allele of the *Cobl* transcription unit. *129Sv* allele is shown in (E), non-mutated *Cast* allele in (F).

Data information: Clones with *Morc1* locus mutations (each assayed in four independent biological replicates) served collectively as control in (E, F), and the clone with the PAS integration (eight independent biological replicates) served as control in (A–D). Visualization of DamID data in all panels is as in Fig 1.

However, the median expression level of the integrated transgenes inside LADs still ranks approximately in the upper 97th percentile of all active endogenous genes (Fig 8E). Thus, even within LADs, most of the integrated transgenes are expressed at very high levels. These expression levels can be sufficient to reduce NL interactions, but only moderately and locally.

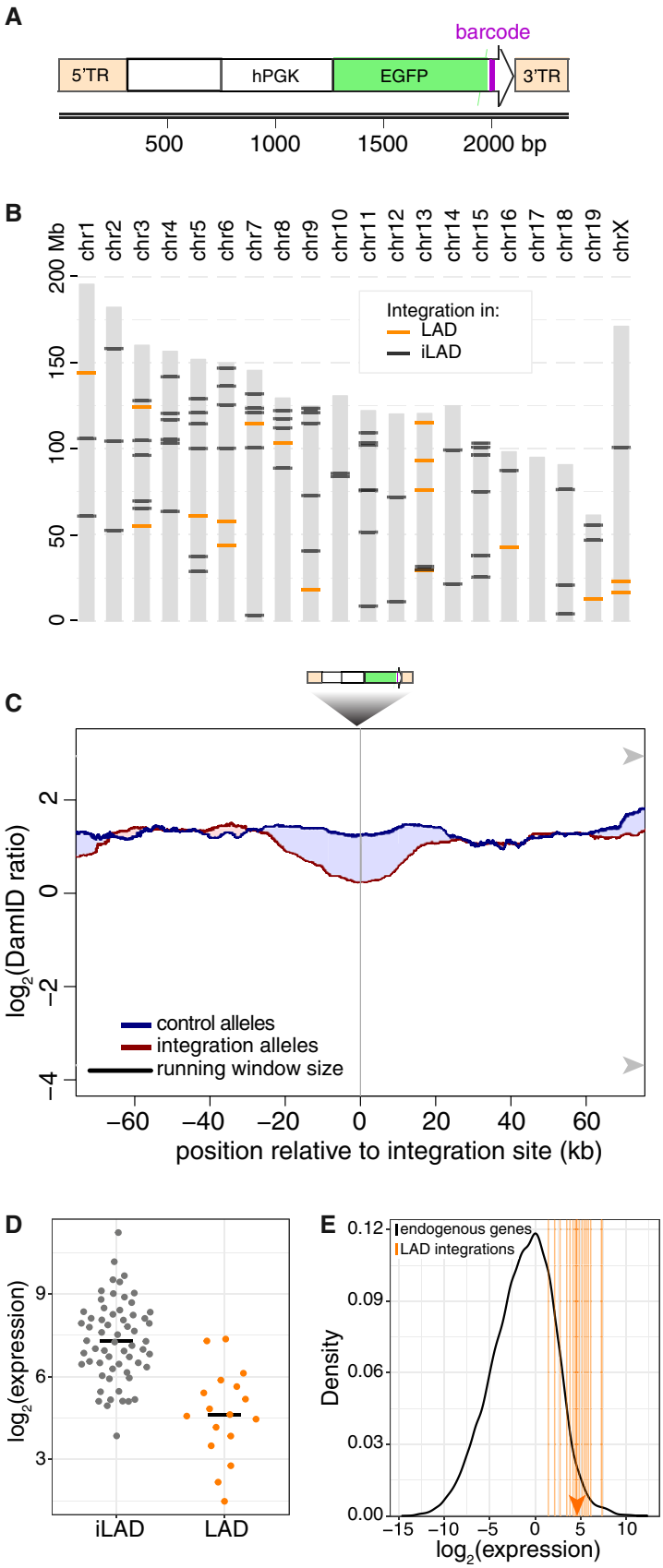

Figure 8.

Figure 8. Effects of a highly active integrated transgene on NL interactions in mES cells.

A Design of the transgene construct, consisting of an enhanced green fluorescent protein (EGFP) transcript, marked at its 3′ end by a random barcode (purple bar) and driven by the human *PGK* promoter. The construct is flanked by the terminal repeats (5′TR and 3′TR) of the *Piggybac* transposon that are used for random integration in the genome.

B Summary of the mapped locations of integrations in the genomes of two F1 hybrid mES cell clonal cell lines. LAD and iLAD integrations are shown in orange and black, respectively.

C Average DamID profiles across 17 transgene integration sites inside LADs. Blue curve shows alleles without integrations; red curve shows the corresponding alleles with integrations. Shading between the lines shows which curve has the highest value.

D Relative expression levels of individual barcoded transgenes in LADs and iLADs.

E Estimated expression levels of integrated transgenes in LADs (vertical orange lines; median value indicated by arrowhead), compared to the distribution of expression levels of all active endogenous genes (black curve).

Discussion

Evidence that components of the transcription machinery can affect the spatial organization of the genome is accumulating, but the underlying processes are still poorly understood (van Steensel & Furlong, 2019; Vermunt *et al*, 2019). The data presented here consistently show that activation of genes in LADs leads to detachment from the NL and conversely that inactivation can lead to increased NL contacts. Moreover, the results point to a remarkable flexibility of the chromatin fiber, allowing for the repositioning of individual genes without much effect on flanking DNA.

Several of our results point to a role for transcription elongation in counteracting NL interactions. First, activity-induced detachment from the NL generally extends across the entire activated transcription unit, from the activated promoter until the 3′ end of the gene. We observed this for a wide range of gene sizes. A role for elongation is also strongly supported by premature termination of the active *Cobl* gene by insertion of a PAS, which primarily caused an increase of NL interactions downstream but not upstream of the new termination site. These results are consistent with a study of the *ThymoD* non-coding RNA gene in mouse T-cell progenitors, where insertion of a PAS prevented detachment from the NL as observed by FISH (Isoda *et al*, 2017). Conversely, read-through transcription into heterochromatin, elicited by influenza virus NS1 protein, was found to cause relocation from the heterochromatic compartment "B" to the euchromatic compartment "A" (Heinz *et al*, 2018), which largely correspond to LADs and iLADs, respectively (van Steensel & Belmont, 2017). How transcription elongation may prevent NL interactions remains to be elucidated. It could be a physical effect, for example when a transcribed gene is tethered to a structure in the nuclear interior. It may also be a biochemical effect, such as the removal of particular NL-interacting chromatin proteins by the elongating RNA polymerase complex. We note that our dataset is skewed toward long genes (median length: 366 kb, $n = 14$) compared to the average genome-wide gene length (which is about 10–15 kb); we cannot rule out that smaller genes often behave differently, although our results for *TRAM1L1* and the transgene insertions (both ~2 kb) suggest that transcription-induced detachment of smaller genes from the NL is also mostly limited to a region of several tens of kb around the transcription unit.

Earlier work found that VP16-induced movement of a LacO repeat toward the nuclear interior could not be blocked by elongation inhibitors (Chuang *et al*, 2006). This is not necessarily contradictory to our evidence that supports a role for elongation; it is possible that a transcription activator like VP16 also promotes detachment from the NL independently of transcription elongation. In support of such an additional mechanism, some of the genes that we studied (e.g., Figs 1A and 2A, and 6A) showed the strongest loss of NL interactions near their 5′ end. Similarly, a class of naturally active genes inside LADs exhibits more prominent detachment of their TSS compared to the downstream transcription units (preprint: Luperchio *et al*, 2017; Wu & Yao, 2017; Leemans *et al*, 2019). Furthermore, global tethering of VP64 across all LADs caused virtually no changes in transcription yet triggered loosening of LAD-NL interactions (Kind *et al*, 2013), underscoring that VP16 can counteract NL interactions without activating transcription.

That detachment from the NL can involve non-transcribed regions is also suggested by our study of the *PTN* gene. CRISPRa of this gene causes detachment that extends several hundred kb into the neighboring *DGKI* gene, even though the latter gene is not detectably activated. Furthermore, the transcriptionally inactivated *Dppa2/4* genes remained mostly dissociated from the NL (Fig 7A). In two earlier reports, relocation from the NL to the nuclear interior was also achieved by tethering of an artificial peptide that induces chromatin decondensation without detectable recruitment of RNA polymerase II (Chuang *et al*, 2006; Therizols *et al*, 2014). It is not understood how this peptide (which is not derived from a naturally occurring protein) exerts this effect, but it suggests that a transcription-independent mechanism of relocation exists in addition to transcription-linked mechanisms. Recent evidence suggests that active chromatin marks such as H3K27ac deposited by p300 may counteract NL interactions (Cabianca *et al*, 2019).

In most cases, the transcriptionally inactive regions adjacent to our activated genes remain relatively unaffected in their NL contacts. Conversely, inhibition of transcription (either by deleting promoters or by insertion of a PAS) leads to increased NL interactions in a very local manner. The latter results were obtained in genomic regions that are facultative LADs, i.e., they may have an intrinsic ability to interact with the NL in the absence of transcription. Genes in constitutive iLADs may lack this ability, either due to spatial constraints or because they lack certain sequence features or chromatin characteristics. It will be of interest to further dissect the molecular mechanisms that underlie the apparent competition between forces that tether chromatin to the NL and forces (such as transcription elongation) that counteract these interactions.

These and previously reported data (Gonzalez-Sandoval & Gasser, 2016; van Steensel & Belmont, 2017; de Leeuw *et al*, 2018; Kim *et al*, 2019; Lochs *et al*, 2019) together suggest a balancing act between transcription and LADs: For many genes, LADs pose a repressive environment (Leemans *et al*, 2019). This, however, may be overcome by strong transcription activators. Once transcription is active, it causes detachment of the gene from the NL. Possibly this

helps to reinforce the active state. It was previously found that a transiently activated gene can remain detached from the NL for several days after the activation signal has subsided (Therizols *et al*, 2014).

We observed changes from late to early replication timing for all five upregulated genes that we assayed by Repli-Seq. The regions that exhibit shifts in replication timing are roughly 1–2 Mb long, matching in size with the usual span of replication domains observed *in vivo* (Hiratani *et al*, 2008; Pope *et al*, 2014). This suggests that there may be a fundamental minimal size of such domains. This is different from the regions that change NL interactions, which can be smaller. Indeed, the overlap between changes in NL interactions and changes in replication timing, while substantial, was imperfect in most instances. The shifts in replication timing tended to involve a larger region than the shift in NL interactions and were centered around the targeted promoters rather than the entire transcription unit. An exception to this is the PTN locus, where changes in NL interactions and replication timing roughly coincide; this may be due to the putative transcription-independent mechanism discussed above. Together, these results suggest that both NL interactions and replication timing can be modulated by the transcription machinery, but elongation appears to play a more prominent role in counteracting NL interactions, while a signal emanating from activated promoters may evoke a change in replication timing. These distinct but closely linked mechanisms may explain why LADs and late-replicating domains overlap strongly but imperfectly. Together, the large datasets presented here provide a wealth of information on the spatial rewiring of chromosomes in response to transcription activation or inactivation.

Materials and Methods

Cell culture

The RPE-1 cell line stably expressing SunTag-CRISPRa (Tame *et al*, 2017) was kindly provided by the R. Medema lab (Netherlands Cancer Institute, Amsterdam) and cultured in DMEM-F12 supplemented with 10% FCS. F121-9 mES cells were kindly provided by J. Gribnau (Erasmus Medical Center, Rotterdam, the Netherlands) and cultured in feeder-free 2i medium according to the 4D Nucleome protocol (https://data.4dnucleome.org/protocols/cb03c0c6-4ba6-4bbe-9210-c430ee4fdb2c/).

Primers

Primer sequences are listed in Tables 2 and 3.

TALE-VP64 experiments

TALE-VP64 constructs (Therizols *et al*, 2014) with Puro resistance marker were kindly provided by Pierre Therizols. The *Sox6* TALE target coordinate is chr7: 116034554–116034570, and the *Nrp1* TALE target coordinate is chr8:128358929–128358945 (mm10 coordinates).

F121-9 cells were transfected with TALE-VP64 constructs targeting *Nrp1* or *Sox2* by electroporation using Lonza Mouse Embryonic Stem Cell Nucleofector™ Kit (VPH-1001) according to the manufacturer's instructions. Cells were selected with Puromycin (1 μg/μl) for 1 week to obtain stable polyclonal cell pools.

Table 2. Miscellaneous primers used.

Oligonucleotide ID	Sequence (5′–3′)
lb877	GACATGGTGCTTGTTGTCCTC
lb982	CTGAGAACGCAGAAGGCTGT
lb991	CTGTTGTCCCACGCATACAG
lb1010	CTGGACCCACCAACTTTGTGG
EB66	CGACAACCACTACCTGAGCA
EB38	CGAACTCCAGCAGGACCATGT
JOYC231	CTCCACTTCCCTCCACCTCT
JOYC232	GAGAGCTTGAACGAAAAACCA
lb563_enrichm_R	CATTGACAAGCACGCCTCAC
lb564_enrichm_F	TAAACCTCGATATACAGACC
lb565_Badapter_ME_5TR_r	GTCTCGTGGGCTCGGAGATGTGTATAAGAGAC AGCAATTTTACGCAGACTATCTTTCTAG
lb566_Badapter_ME_3TR_f	GTCTCGTGGGCTCGGAGATGTGTATAAGAG ACAGGTACGTCACAATATGATTATCTTTCTAG

Table 3. Primers for RT–qPCR.

Target gene	Oligonucleotide ID	Sequence (5′–3′)
ABCB1	lb667_ABCB1_hs_qPCR_f	CAGTTGAGTGGTGGGCAGAA
	lb668_ABCB1_hs_qPCR_r	GCCTTATCCAGAGCCACCTG
ZNF804B	lb669_ZNF804B_hs_qPCR_f	GCAATCTGAATGTGTTTCTGGA
	lb670_ZNF804B_hs_qPCR_r	ATTCCTTGCTGGAGTTGCT
PTN	lb671_PTN_hs_qPCR_f	CCCAAACCTCAAGAGAAGG
	lb672_PTN_hs_qPCR_r	ACCATCTTCTCAAACTCTCC
SOX6	lb673_SOX6_hs_qPCR_f	TACCAACACTTGTCAGTACCA
	lb674_SOX6_hs_qPCR_r	TCTCTGATTCCATTCTTTGCTG
TRAM1L1	lb675_TRAM1L1_hs_qPCR_f	TCACTGTTGGGTTTCACCT
	lb676_TRAM1L1_hs_qPCR_r	TTTCCAGTAAGGGCATCAG
NLGN1	lb817_qPCR_NLGN1_hs_f	GGTTTCTTGAGTACAGGCG
	lb818_qPCR_NLGN1_hs_r	TGTATGAGATCAAGGAGTCCA
MLK4	lb821_qPCR_KIAA1804_hs_f	GAGGAAGGGCAAGTTTAAGAG
	lb822_qPCR_KIAA1804_hs_r	TTGTGCTGGAAATCTGAAGG
SLC35F3	lb823_qPCR_SLC35F3_hs_f	TTGCCGTTACATATCCCAC
	lb824_qPCR_SLC35F3_hs_r	TGGTGTAGTGATCAATCACTG
ADAM22	lb829_qPCR_ADAM22_hs_f	GTTACTACCAGGGCCATATCC
	lb830_qPCR_ADAM22_hs_r	AGAACATCCCATGAAGTCCG

CRISPRa experiments

sgRNAs were cloned into LentiGuide-Puro vector (Addgene #52963) using restriction enzyme BsmBI, and lentivirus was prepared. RPE-1 cells stably expressing SunTag-CRISPRa were infected with LentiGuide virus and selected with 10 μg/μl puromycin for 1 week to obtain stable polyclonal cell pools.

PAS integration

A PAS was inserted by in-frame integration of a blasticidin resistance (BlastR) cassette followed by the PAS into the *Cobl* gene. For this purpose, sgRNA sequence AGTCATCTGTGCGAAGTGTG was cloned into Blast-TIA vector (Lackner *et al*, 2015) (kindly supplied by the Brummelkamp lab, Netherlands Cancer Institute) via BbsI restriction digestion. Cells were transfected with the resulting Blast-TIA vector co-transfected with Cas9 expression vector pX330 (Addgene #42230) by nucleofection and subjected to selection by culturing in the presence of 10 μg/μl blasticidin for 1 week. Clones were picked and screened for correct integration of the BlastR cassette by PCR with primers lb877 and lb982. Heterozygosity of the integration was confirmed by PCR using primers lb982 and lb991, and the *129Sv* allele was identified as the targeted allele by PCR using primers lb877 and lb1010, followed by Sanger sequencing with the same primers.

Repli-seq

Repli-seq was performed as described (Marchal *et al*, 2018). Sequencing was done on a NovaSeq 6000 system (Illumina), 50-bp read length.

mRNA-seq

As previously described (Gogola *et al*, 2018), mRNA-seq was performed as follows. Quality and quantity of the total RNA were assessed by the 2100 Bioanalyzer using a Nano chip (Agilent, Santa Clara, CA). Total RNA samples having RIN>8 were subjected to library generation. Strand-specific libraries were generated using the TruSeq Stranded mRNA sample preparation kit (Illumina Inc., San Diego, RS-122-2101/2) according to the manufacturer's instructions (Illumina, Part # 15031047 Rev. E). Briefly, polyadenylated RNA from intact total RNA was purified using oligo-dT beads. Following purification, the RNA was fragmented, random-primed, and reverse-transcribed using SuperScript II Reverse Transcriptase (Invitrogen, part # 18064-014) with the addition of actinomycin D. Second-strand synthesis was performed using polymerase I and RNaseH with replacement of dTTP for dUTP. The generated cDNA fragments were 3′ end adenylated and ligated to Illumina paired-end sequencing adapters and subsequently amplified by 12 cycles of PCR. The libraries were analyzed on a 2100 Bioanalyzer using a 7500 chip (Agilent, Santa Clara, CA), diluted and pooled equimolar into a multiplex sequencing pool, and stored at −20°C. The libraries were sequenced with 65 base single reads on a HiSeq2500 using V4 chemistry (Illumina Inc., San Diego). Reads were aligned to hg19 or mm10 using TopHat version 2.1, with Ensembl genome build 75. For *Cobl* PAS integration experiments in the F1 hybrid ES cells, mRNA-seq reads were aligned to mm10 using STAR (Dobin *et al*, 2013).

RT–qPCR

Cells were collected in TRIsure and total RNA was extracted using PureLink RNA Mini Kit (Thermo Fisher Scientific) according to the manufacturer's instructions. RNA was reverse-transcribed using Tetro Reverse Transcriptase (Bioline) with Oligo(dT)20 primers (Thermo Fisher Scientific) according to the manufacturer's instructions. qPCR was performed using SensiFast no-ROX mix (Bioline) in a 10 μl reaction. Primers are listed in Table 3.

Generation and mapping of random integrations

The hPGK-EGFP cassette was derived from TRIP vector pPTK-Gal4-mPGK-Puro-IRES-eGFP-sNRP-pA (Akhtar *et al*, 2014) by replacing mPGK-Puro-IRES with the human PGK promoter using restriction enzyme cloning with SalI and NcoI. Generation of a barcoded plasmid pool and integration into F121-9 mES cells was performed as described (Akhtar *et al*, 2014). Clones with high EGFP expression were sorted by FACS and screened for high integration copy number by qPCR with EGFP-specific primers EB66 and EB38, using *Lbr*-specific primers (JOYC231 and JOYC232) for normalization.

Mapping of integrations without linking to barcodes was done by Tagmentation as described (preprint: Stern, 2017) with minor modifications: Before PCR for Tn5 adapters, linear amplification of PiggyBac integrations was performed using primers lb565 or lb566 for mapping in reverse or forward orientation respectively. Linear amplification was performed using 0.5 U Phusion polymerase (Bioline) in a 20 μl reaction with Phusion GC-rich buffer, 1 mM dNTPs, 50 nM primer. Reaction was incubated at 98°C for 30 s, then 45 cycles of 98°C for 8 s, 60°C for 5 s and 72°C for 30 s followed by a final step at 72°C for 20 s. For PCR amplification, PiggyBac-specific primers lb565 or 566 were used for mapping in reverse or forward orientation, respectively.

To process the tagmentation mapping reads, the Tn5 adaptor sequence and PiggyBac primer sequence at the ends of the paired-end reads were removed using an adaptation of *cutadapt v1.11*. The genomic part of the sequence was mapped to strain-specific versions of GRCm38 release 68 from Ensembl using *bowtie v2.3.4.1* with mapping set to "*very-sensitive*". To create these strain-specific genomes, SNP information was downloaded from the Mouse Genomes Project (Keane *et al*, 2011; http://www.sanger.ac.uk/science/data/mouse-genomes-project) as VCF files "CAST_EiJ.mgp.v5.snps.dbSNP142.vcf.gz" and "129S1_SvImJ.mgp.v5.snps.dbSNP142.vcf.gz" (version 1 May 2015). *Bcftools* was used to incorporate all SNPs into the GRCm38 reference genome. After mapping to strain-specific genomes, bam files were compared, and for each read, the alignment with the highest alignment score (AS) was used. When the AS was identical, a random choice was made. Read-pairs aligning in opposite orientation and <1,500 bp apart were converted to genomic regions using the *bamToBed* from *bedtools* and *awk*, covering both reads as well as the region in between. *Genomecov* from *bedtools* and *awk* was used to combine regions and calculate coverage. Integration sites were called by combining regions from PCRs from both transposon arms using *closest* from *bedtools* and *awk*. Regions on opposite strands that were at most 5 bp apart were regarded to represent an integration. Next, the allele of the integration was determined by using *mpileup* from *Samtools* (Li *et al*, 2009) *v1.5* with a maximum depth of 50 to count the number of mismatch positions over the complete region compared to both of the strain-specific GRCm38 modifications. Each position with the allele of the strain-specific genome occurring in a ratio < 0.5 was considered a mismatch position. The allele with the lowest number of mismatch positions was then considered the allele of integration. In case of equal number of mismatch positions, the integration allele

was classified as ambiguous. We selected only putative integration sites with at least 1 read having a mapping quality > 10 and > 500 reads mapped on both sides of it.

In addition, allele-specific mapping of the integrations and linking to their barcodes was performed by inverse PCR as described (Akhtar *et al*, 2014), except that the mapping of reads was confined to regions that were initially found by tagmentation mapping. Tagmentation alone identified 50 integrations for clone CM1407 and 56 for clone CM1420, of which 37 and 43 were linked to a single, unique barcode, respectively.

Expression analysis of ES cell clones with random integrations

Clones CM1407 and CM1420 were subjected to mRNA-seq as above. For comparison between eGFP and endogenous mRNA expression, a fasta entry for eGFP was added to the mouse genome version mm10 chromosomes 1-19, X, Y, and M without alternative contigs. The annotation of eGFP transcript was also added to gencode version M18. STAR (Dobin *et al*, 2013) version 2.6.0c was used to align the cDNA reads to this modified reference genome, and for each transcript, reads were counted. DESeq2 (Love *et al*, 2014) was used to calculate fragments per kilobase million (FPKM) values for each gene, including eGFP.

In addition, barcode-specific expression was determined using sequencing of the barcodes in cDNA similar to the standard TRIP protocol (Akhtar *et al*, 2014). To discriminate between genuine barcodes and sequencing errors of these barcodes, *starcode* (Zorita *et al*, 2015) was used. Unlike the standard TRIP protocol, reads were not normalized by gDNA counts. Finally, the eGFP FPKM was scaled by the number of integrations for each clone in order to determine the average eGFP expression per integrated reporter. These numbers were 52 for clone CM1417 and 55 for clone CM1420; barcodes were counted 2 times when found at 2 integration sites.

Lamina-associated domains coordinates in mouse ES cells were obtained from Peric-Hupkes *et al* (2010) and adjusted to mm10 using the LiftOver tool (Hinrichs *et al*, 2006). To estimate FPKM's for integrations in LADs and iLADs separately, barcodes were used that had a unique location according to a combination of iPCR and tagmentation mapping. In total, 17 barcodes could be confidently linked to LAD locations. To determine LAD and iLAD-specific expression levels, the average eGFP FPKM per integration was scaled by the median LAD and iLAD expression. Finally, the percentile of eGFP FPKM relative to endogenous active genes was calculated by counting the number of genes with higher FPKM than the eGFP estimation, divided by the total number of active genes (defined as genes with FPKM > 0).

DamID-seq

DamID-seq was performed as described (Brueckner *et al*, 2016) with minor modifications. Dam fused to human LMNB1 protein (Dam-LMNB1) or unfused Dam were expressed in cells by lentiviral transduction (Vogel *et al*, 2007). Three days after infection, cells were collected for genomic DNA (gDNA) isolation. gDNA was pre-treated with SAP (10 U, New England Biolabs #M0371S) in CutSmart buffer in a total volume of 10 µl at 37°C for 1 h, followed by heat inactivation at 65°C for 20 min to suppress signal from apoptotic fragments. This gDNA was then digested with DpnI (10 U, New England Biolabs #R0176L) in CutSmart buffer in a total volume of 10 µl at 37°C for 8 h followed by heat inactivation at 80°C for 20 min. Fragments were ligated to 12.5 pmol DamID adapters using T4 ligase (2.5 U, Roche #10799009001) in T4 ligase buffer in a total volume of 20 µl incubated at 16°C for 16 h. The reaction was heat-inactivated for 10 min at 65°C. Products were then digested with DpnII to destroy partially methylated fragments. DpnII buffer and DpnII (10 U, New England Biolabs #R0543L) were added in a total volume of 50 µl and incubated at 37°C for 1 h. Next, 8 µl of DpnII-digested products was amplified by PCR with MyTaq Red Mix (Bioline #BIO-25044) and 1.25 µM primers Adr-PCR-Rand1 in a total volume of 40 µl. PCR settings were 8 min at 72°C (1×) followed by 20 s at 94°C, 30 s at 58°C, 20 s at 72°C (24× for Dam, 28× for Dam-LMNB1 samples) and 2 min at 72°C (1×). Remaining steps were performed as previously described. Samples were sequenced on an Illumina HiSeq2500.

Processing of RPE-1 and ES cell DamID data

First, the constant DamID adapter was trimmed from the 65-bp single-end reads using *cutadapt* (Martin, 2011) version 1.11 and custom scripts. The remaining sequence starting with GATC was mapped to hg19 with bowtie2 (Langmead & Salzberg, 2012) version 2.2.6. Uniquely mapped reads (filtered for bowtie's XS-tag) were then assigned to individual gDNA sequences between two GATC motifs (referred to as GATC fragments), which are the units of further data processing and analysis because Dam-only methylates GATC motifs. Further processing and analysis were done in R (R Core Team, 2017) versions 3.4–3.6 using Bioconductor (Huber *et al*, 2015), in particular the packages GenomicRanges (Lawrence *et al*, 2013) and Sushi (Phanstiel *et al*, 2014).

Replicate experiments were combined by summing the reads for each GATC fragment. Hence, experiments with more reads were weighed proportionally stronger than experiments with fewer reads. Extremely high read counts of individual GATC fragments (> 100 times the genome-wide average) were assumed to be due to PCR artifacts; these read counts were replaced with the genome-wide average read count. Next, smoothing was applied by summing read counts over a running window of 201 consecutive GATC fragments. A pseudocount of 30 was added to each window. The ratio Dam-lamin B1/Dam-only was calculated for each window and $\log_2$-transformed. Finally, the $\log_2$ ratios were normalized by subtracting the genome-wide average $\log_2$ ratio.

When comparing experimental and control DamID log ratios in genome-wide scatterplots, we noticed modest systematic biases and skews (visible as point clouds that were somewhat banana-shaped rather than cigar-shaped) or differences in the dynamic ranges of the DamID values that are likely to be of technical nature (under the assumption that CRISRPa activation of a single gene is unlikely to cause a genome-wide systematic effect). We estimated such skews empirically by applying a lowess fit (span = 0.5) to the experimental ~ control comparison of a random selection of 50,000 GATC fragments and then used this fit to correct the genome-wide comparison. This effectively removed genome-wide biases, thereby enhancing the sensitivity to detect local changes in NL contacts around the targeted genes.

Processing of F1 hybrid mouse ES cell DamID data

For DamID on F1 hybrid *129/Cast* mouse ES cells, 150 or 200 nt single reads were trimmed to remove the DamID adaptor sequence and then strain-specifically mapped to mm10 with WASP (van de Geijn *et al*, 2015) using bowtie2 and VCF files from the mouse genomes project (Keane *et al*, 2011; https://www.sanger.ac.uk/science/data/mouse-genomes-project; version 5). Data were further processed as described for RPE-1 cells, except that a smoothing window size of 301 instead of 201 GATC fragments was applied.

Domainograms

The domainograms in this study are related to those reported previously (de Wit *et al*, 2008; Tolhuis *et al*, 2011), but do not show estimated *P*-values, which are not easily calculated for our experimental design. Rather, for a given window size, they show the ranking of changes in DamID log ratios (experimental minus control) relative to windows of the same size genome-wide. Briefly, in a window of w neighboring GATC fragments, the difference in mean DamID log-ratio is calculated between the experimental and control samples. This is done for all possible windows of size w genome-wide. Next, windows in which both experimental and control sample showed only baseline DamID signals (i.e., both log ratios are in the respective lower 0.3 quantiles genome-wide) are discarded. This is done because baseline fluctuations can appear strong on a logarithmic scale but are generally of minor amplitude on a linear scale and therefore unlikely to be of biological relevance. The remaining windows are ranked by their log-ratio differences; ranks $< 5\%$ or $> 95\%$ are visualized by blue or red color scales, respectively. This is repeated for 28 different window sizes w that are logarithmically ranging from 67 and 2,917 GATC fragments, i.e., from ~30 kb to ~1 Mb.

Data analysis of Repli-seq samples

Repi-seq reads from early and late-replicating fractions were mapped and processed in the same way as DamID reads, using the same smoothing window size. Instead of Dam-lamin B1/Dam-only, the ratio late/early replication was calculated.

Hi-C data analysis

Hi-C data from wild-type RPE-1 cells are from Darrow *et al* (2016) (Data ref: Darrow *et al*, 2016) and visualized using Juicebox 1.8.8 (Durand *et al*, 2016).

Data availability

The datasets (and computer code) produced in this study are available in the following databases:
Sequencing reads and processed data of DamID, Repli-seq and RNA-seq experiments: Gene Expression Omnibus GSE133275 (https://www.ncbi.nlm.nih.gov/geo/query/acc.cgi?acc=GSE133275).
Data analysis code: https://github.com/vansteensellab/LAD_rewiring.

Expanded View for this article is available online.

Acknowledgments
We thank the NKI Genomics, Flow Cytometry, and RHPC core facilities, as well as Tom Rieuwerts and Ludo Pagie for technical assistance and Lorenzo Bombardelli for Tn5 protein. We thank Andrew Belmont, Jian Ma, and other members of the 4DN Center for Nuclear Cytomics for helpful discussions. Supported by NIH Common Fund "4D Nucleome" Program grant U54DK107965 (BvS and DMG) and European Research Council Advanced Grant 694466 (BvS). The Oncode Institute is partly supported by KWF Dutch Cancer Society.

Author contributions
LB: conceived and designed study, conducted majority of experiments, initial data analysis, and wrote manuscript. PAZ: performed Repli-seq experiments and initial Repli-seq data analysis. DP-H: performed experiments and data analysis. TS: processing of DamID data. CL: performed data analysis. JS: *Morc1* locus deletions and initial data analysis. DMG: supervised Repli-seq experiments, generation of *Morc1* locus deletions and initial data analysis. BS: designed study, performed coding and data analysis, wrote manuscript, and supervised project.

Conflict of interest
The authors declare that they have no conflict of interest.

References

Akhtar W, Pindyurin AV, de Jong J, Pagie L, Ten Hoeve J, Berns A, Wessels LF, van Steensel B, van Lohuizen M (2014) Using TRIP for genome-wide position effect analysis in cultured cells. *Nat Protoc* 9: 1255 – 1281

Brueckner L, van Arensbergen J, Akhtar W, Pagie L, van Steensel B (2016) High-throughput assessment of context-dependent effects of chromatin proteins. *Epigenetics Chromatin* 9: 43

Cabianca DS, Munoz-Jimenez C, Kalck V, Gaidatzis D, Padeken J, Seeber A, Askjaer P, Gasser SM (2019) Active chromatin marks drive spatial sequestration of heterochromatin in *C. elegans* nuclei. *Nature* 569: 734 – 739

Chen H, Zheng X, Zheng Y (2014) Age-associated loss of lamin-B leads to systemic inflammation and gut hyperplasia. *Cell* 159: 829 – 843

Chuang CH, Carpenter AE, Fuchsova B, Johnson T, de Lanerolle P, Belmont AS (2006) Long-range directional movement of an interphase chromosome site. *Curr Biol* 16: 825 – 831

Darrow EM, Huntley MH, Dudchenko O, Stamenova EK, Durand NC, Sun Z, Huang SC, Sanborn AL, Machol I, Shamim M *et al* (2016) Deletion of DXZ4 on the human inactive X chromosome alters higher-order genome architecture. *Proc Natl Acad Sci USA* 113: E4504 – E4512

Darrow EM, Huntley MH, Lieberman Aiden E (2016) Gene Expression Omnibus GSE71831 (https://www.ncbi.nlm.nih.gov/geo/query/acc.cgi?acc=GSE71831). [DATASET]

Dialynas G, Speese S, Budnik V, Geyer PK, Wallrath LL (2010) The role of *Drosophila* Lamin C in muscle function and gene expression. *Development* 137: 3067 – 3077

Dixon JR, Selvaraj S, Yue F, Kim A, Li Y, Shen Y, Hu M, Liu JS, Ren B (2012) Topological domains in mammalian genomes identified by analysis of chromatin interactions. *Nature* 485: 376 – 380

Dobin A, Davis CA, Schlesinger F, Drenkow J, Zaleski C, Jha S, Batut P, Chaisson M, Gingeras TR (2013) STAR: ultrafast universal RNA-seq aligner. *Bioinformatics* 29: 15 – 21

Durand NC, Robinson JT, Shamim MS, Machol I, Mesirov JP, Lander ES, Aiden EL (2016) Juicebox provides a visualization system for Hi-C contact maps with unlimited zoom. *Cell Syst* 3: 99 – 101

Filion GJ, van Bemmel JG, Braunschweig U, Talhout W, Kind J, Ward LD, Brugman W, de Castro IJ, Kerkhoven RM, Bussemaker HJ *et al* (2010) Systematic protein location mapping reveals five principal chromatin types in *Drosophila* cells. *Cell* 143: 212 – 224

Finlan LE, Sproul D, Thomson I, Boyle S, Kerr E, Perry P, Ylstra B, Chubb JR, Bickmore WA (2008) Recruitment to the nuclear periphery can alter expression of genes in human cells. *PLoS Genet* 4: e1000039

van de Geijn B, McVicker G, Gilad Y, Pritchard JK (2015) WASP: allele-specific software for robust molecular quantitative trait locus discovery. *Nat Methods* 12: 1061 – 1063

Gogola E, Duarte AA, de Ruiter JR, Wiegant WW, Schmid JA, de Bruijn R, James DI, Guerrero Llobet S, Vis DJ, Annunziato S *et al* (2018) Selective loss of PARG restores PARylation and counteracts PARP inhibitor-mediated synthetic lethality. *Cancer Cell* 33: 1078 – 1093.e1012

Gonzalez-Sandoval A, Gasser SM (2016) On TADs and LADs: spatial control over gene expression. *Trends Genet* 32: 485 – 495

Greil F, Moorman C, van Steensel B (2006) DamID: mapping of *in vivo* protein-genome interactions using tethered DNA adenine methyltransferase. *Methods Enzymol* 410: 342 – 359

Guelen L, Pagie L, Brasset E, Meuleman W, Faza MB, Talhout W, Eussen BH, de Klein A, Wessels L, de Laat W *et al* (2008) Domain organization of human chromosomes revealed by mapping of nuclear lamina interactions. *Nature* 453: 948 – 951

Harr JC, Luperchio TR, Wong X, Cohen E, Wheelan SJ, Reddy KL (2015) Directed targeting of chromatin to the nuclear lamina is mediated by chromatin state and A-type lamins. *J Cell Biol* 208: 33 – 52

Heinz S, Texari L, Hayes MGB, Urbanowski M, Chang MW, Givarkes N, Rialdi A, White KM, Albrecht RA, Pache L *et al* (2018) Transcription elongation can affect genome 3D structure. *Cell* 174: 1522 – 1536.e1522

Hinrichs AS, Karolchik D, Baertsch R, Barber GP, Bejerano G, Clawson H, Diekhans M, Furey TS, Harte RA, Hsu F *et al* (2006) The UCSC genome browser database: update 2006. *Nucleic Acids Res* 34: D590 – D598

Hiratani I, Ryba T, Itoh M, Yokochi T, Schwaiger M, Chang CW, Lyou Y, Townes TM, Schubeler D, Gilbert DM (2008) Global reorganization of replication domains during embryonic stem cell differentiation. *PLoS Biol* 6: e245

Huber W, Carey VJ, Gentleman R, Anders S, Carlson M, Carvalho BS, Bravo HC, Davis S, Gatto L, Girke T *et al* (2015) Orchestrating high-throughput genomic analysis with Bioconductor. *Nat Methods* 12: 115 – 121

Isoda T, Moore AJ, He Z, Chandra V, Aida M, Denholtz M, Piet van Hamburg J, Fisch KM, Chang AN, Fahl SP *et al* (2017) Non-coding transcription instructs chromatin folding and compartmentalization to dictate enhancer-promoter communication and T cell fate. *Cell* 171: 103 – 119.e118

Keane TM, Goodstadt L, Danecek P, White MA, Wong K, Yalcin B, Heger A, Agam A, Slater G, Goodson M *et al* (2011) Mouse genomic variation and its effect on phenotypes and gene regulation. *Nature* 477: 289 – 294

Kim Y, Zheng X, Zheng Y (2019) Role of lamins in 3D genome organization and global gene expression. *Nucleus* 10: 33 – 41

Kind J, Pagie L, Ortabozkoyun H, Boyle S, de Vries SS, Janssen H, Amendola M, Nolen LD, Bickmore WA, van Steensel B (2013) Single-cell dynamics of genome-nuclear lamina interactions. *Cell* 153: 178 – 192

Kind J, Pagie L, de Vries SS, Nahidiazar L, Dey SS, Bienko M, Zhan Y, Lajoie B, de Graaf CA, Amendola M *et al* (2015) Genome-wide maps of nuclear lamina interactions in single human cells. *Cell* 163: 134 – 147

Kohwi M, Lupton JR, Lai SL, Miller MR, Doe CQ (2013) Developmentally regulated subnuclear genome reorganization restricts neural progenitor competence in *Drosophila*. *Cell* 152: 97 – 108

Kumaran RI, Spector DL (2008) A genetic locus targeted to the nuclear periphery in living cells maintains its transcriptional competence. *J Cell Biol* 180: 51 – 65

Lackner DH, Carre A, Guzzardo PM, Banning C, Mangena R, Henley T, Oberndorfer S, Gapp BV, Nijman SMB, Brummelkamp TR *et al* (2015) A generic strategy for CRISPR-Cas9-mediated gene tagging. *Nat Commun* 6: 10237

Langmead B, Salzberg SL (2012) Fast gapped-read alignment with Bowtie 2. *Nat Methods* 9: 357 – 359

Lawrence M, Huber W, Pages H, Aboyoun P, Carlson M, Gentleman R, Morgan MT, Carey VJ (2013) Software for computing and annotating genomic ranges. *PLoS Comput Biol* 9: e1003118

Leemans C, van der Zwalm MCH, Brueckner L, Comoglio F, van Schaik T, Pagie L, van Arensbergen J, van Steensel B (2019) Promoter-intrinsic and local chromatin features determine gene repression in LADs. *Cell* 177: 852 – 864.e814

de Leeuw R, Gruenbaum Y, Medalia O (2018) Nuclear lamins: thin filaments with major functions. *Trends Cell Biol* 28: 34 – 45

Li H, Handsaker B, Wysoker A, Fennell T, Ruan J, Homer N, Marth G, Abecasis G, Durbin R, Genome Project Data Processing S (2009) The sequence alignment/map format and SAMtools. *Bioinformatics* 25: 2078 – 2079

Lochs SJA, Kefalopoulou S, Kind J (2019) Lamina associated domains and gene regulation in development and cancer. *Cells* 8: E271

Love MI, Huber W, Anders S (2014) Moderated estimation of fold change and dispersion for RNA-seq data with DESeq2. *Genome Biol* 15: 550

Lund E, Oldenburg AR, Delbarre E, Freberg CT, Duband-Goulet I, Eskeland R, Buendia B, Collas P (2013) Lamin A/C-promoter interactions specify chromatin state-dependent transcription outcomes. *Genome Res* 23: 1580 – 1589

Luperchio TR, Sauria MEG, Wong X, Gaillard MC, Tsang P, Pekrun K, Ach RA, Yamada NA, Taylor J, Reddy KL (2017) Chromosome conformation paints reveal the role of lamina association in genome organization and regulation. *bioRxiv* https://doi.org/10.1101/122226 [PREPRINT]

Marchal C, Sasaki T, Vera D, Wilson K, Sima J, Rivera-Mulia JC, Trevilla-Garcia C, Nogues C, Nafie E, Gilbert DM (2018) Genome-wide analysis of replication timing by next-generation sequencing with E/L Repli-seq. *Nat Protoc* 13: 819 – 839

Martin M (2011) Cutadapt removes adapter sequences from high-throughput sequencing reads. *EMBnetjournal* 17: 10 – 12

Nora EP, Lajoie BR, Schulz EG, Giorgetti L, Okamoto I, Servant N, Piolot T, van Berkum NL, Meisig J, Sedat J *et al* (2012) Spatial partitioning of the regulatory landscape of the X-inactivation centre. *Nature* 485: 381 – 385

Peric-Hupkes D, Meuleman W, Pagie L, Bruggeman SW, Solovei I, Brugman W, Graf S, Flicek P, Kerkhoven RM, van Lohuizen M *et al* (2010) Molecular maps of the reorganization of genome-nuclear lamina interactions during differentiation. *Mol Cell* 38: 603 – 613

Phanstiel DH, Boyle AP, Araya CL, Snyder MP (2014) Sushi.R: flexible, quantitative and integrative genomic visualizations for publication-quality multi-panel figures. *Bioinformatics* 30: 2808 – 2810

Pope BD, Ryba T, Dileep V, Yue F, Wu W, Denas O, Vera DL, Wang Y, Hansen RS, Canfield TK *et al* (2014) Topologically associating domains are stable units of replication-timing regulation. *Nature* 515: 402 – 405

R Core Team (2017) *R: a language and environment for statistical computing*. R Core Team. https://www.R-projectorg

Reddy KL, Zullo JM, Bertolino E, Singh H (2008) Transcriptional repression mediated by repositioning of genes to the nuclear lamina. *Nature* 452: 243 – 247

Robson MI, de Las Heras JI, Czapiewski R, Le Thanh P, Booth DG, Kelly DA, Webb S, Kerr AR, Schirmer EC (2016) Tissue-specific gene repositioning by muscle nuclear membrane proteins enhances repression of critical developmental genes during myogenesis. *Mol Cell* 62: 834 – 847

Robson MI, de Las Heras JI, Czapiewski R, Sivakumar A, Kerr ARW, Schirmer EC (2017) Constrained release of lamina-associated enhancers and genes from the nuclear envelope during T-cell activation facilitates their association in chromosome compartments. *Genome Res* 27: 1126 – 1138

Shevelyov YY, Lavrov SA, Mikhaylova LM, Nurminsky ID, Kulathinal RJ, Egorova KS, Rozovsky YM, Nurminsky DI (2009) The B-type lamin is required for somatic repression of testis-specific gene clusters. *Proc Natl Acad Sci USA* 106: 3282 – 3287

Sima J, Chakraborty A, Dileep V, Michalski M, Klein KN, Holcomb NP, Turner JL, Paulsen MT, Rivera-Mulia JC, Trevilla-Garcia C *et al* (2019) Identifying cis elements for spatiotemporal control of mammalian DNA replication. *Cell* 176: 816 – 830.e818

van Steensel B, Belmont AS (2017) Lamina-associated domains: links with chromosome architecture, heterochromatin, and gene repression. *Cell* 169: 780 – 791

van Steensel B, Furlong EEM (2019) The role of transcription in shaping the spatial organization of the genome. *Nat Rev Mol Cell Biol* 20: 327 – 337

Stern DL (2017) Tagmentation-based mapping (TagMap) of mobile DNA genomic insertion sites. *bioRxiv* https://doi.org/10.1101/037762 [PREPRINT]

Tame MA, Manjon AG, Belokhvostova D, Raaijmakers JA, Medema RH (2017) TUBB3 overexpression has a negligible effect on the sensitivity to taxol in cultured cell lines. *Oncotarget* 8: 71536 – 71547

Tanenbaum ME, Gilbert LA, Qi LS, Weissman JS, Vale RD (2014) A protein-tagging system for signal amplification in gene expression and fluorescence imaging. *Cell* 159: 635 – 646

Therizols P, Illingworth RS, Courilleau C, Boyle S, Wood AJ, Bickmore WA (2014) Chromatin decondensation is sufficient to alter nuclear organization in embryonic stem cells. *Science* 346: 1238 – 1242

Tolhuis B, Blom M, Kerkhoven RM, Pagie L, Teunissen H, Nieuwland M, Simonis M, de Laat W, van Lohuizen M, van Steensel B (2011) Interactions among Polycomb domains are guided by chromosome architecture. *PLoS Genet* 7: e1001343

Tumbar T, Belmont AS (2001) Interphase movements of a DNA chromosome region modulated by VP16 transcriptional activator. *Nat Cell Biol* 3: 134 – 139

Vermunt MW, Zhang D, Blobel GA (2019) The interdependence of gene-regulatory elements and the 3D genome. *J Cell Biol* 218: 12 – 26

Vogel MJ, Peric-Hupkes D, van Steensel B (2007) Detection of *in vivo* protein-DNA interactions using DamID in mammalian cells. *Nat Protoc* 2: 1467 – 1478

de Wit E, Braunschweig U, Greil F, Bussemaker HJ, van Steensel B (2008) Global chromatin domain organization of the *Drosophila* genome. *PLoS Genet* 4: e1000045

Wu F, Yao J (2017) Identifying novel transcriptional and epigenetic features of nuclear lamina-associated genes. *Sci Rep* 7: 100

Zorita E, Cusco P, Filion GJ (2015) Starcode: sequence clustering based on all-pairs search. *Bioinformatics* 31: 1913 – 1919